Applied Catalysis B: Environmental 172–173 (2015) 116–128

Contents lists available at ScienceDirect

Applied Catalysis B: Environmental

journal homepage: www.elsevier.com/locate/apcatb

Bi-functional hydrotalcite-derived NiO–CaO–Al_2O_3 catalysts for steam reforming of biomass and/or tar model compound at low steam-to-carbon conditions

J. Ashok, Y. Kathiraser, M.L. Ang, S. Kawi*

Department of Chemical and Biomolecular Engineering, National University of Singapore, Singapore 119260, Republic of Singapore

ARTICLE INFO

Article history:
Received 13 October 2014
Received in revised form 12 February 2015
Accepted 14 February 2015
Available online 17 February 2015

Keywords:
Hydrotalcite
Steam reforming
Biomass
Tars
NiO–CaO–Al_2O_3

ABSTRACT

In this paper, the bi-functional properties of NiO–CaO–Al_2O_3 (Ni–Ca–Al) catalysts derived from hydrotalcite-like precursors were explored for steam reforming of toluene and biomass reactions. The influence of CO_2 sorption property of NiO–CaO–Al_2O_3 catalysts was also explored by changing Ca/Al molar composition ratio for steam reforming reaction. The steam reforming of toluene reaction was investigated at low steam-to-carbon conditions (S/C = 1). An optimum catalyst composition of Ni–Ca–Al(8:62:30) gave superior catalytic performance in terms of stability and activity in both the reforming reactions. At S/C value of 1, Ni–Ca–Al(8:62:30) catalyst displayed a stable toluene conversion of near 70% for a period of 24 h tested in toluene reforming reaction. At 650 °C, about 85% of biomass was converted to gaseous products over Ni–Ca–Al(8:62:30), which is the highest among all the catalysts tested. The XRD analysis of reduced and spent catalysts shows that the rate of agglomeration of active metallic Ni species over Ni–Ca–Al(8:62:30) catalyst is considerably lesser when compared to other catalysts. The TPR and XPS analyses reveals that the calcined and reduced Ni–Ca–Al catalysts are in Ca(Ni, Al)O solid solution form, respectively. CO_2– TPD studies shows that the basicity of Ni–Ca–Al(8:62:30) catalyst is higher compared to other Ni–Ca–Al catalysts. The rate of carbon deposition over Ni–Ca–Al(8:62:30) catalyst during steam reforming of toluene reaction is 2.5 mgC g^{-1} h^{-1}, which is also the lowest among all the catalysts. Hence, the low carbon deposition rate is one of the reasons for its stable catalytic performance compared to the rest.

© 2015 Elsevier B.V. All rights reserved.

1. Introduction

Catalytic steam reforming of biomass to produce H_2-rich synthesis gas is an increasingly attractive option because of the rising interest in utilizing biomass derived from forest, agricultural, and municipal solid waste materials. Biomass is also considered as a CO_2 neutral source of renewable energy [1–5]. However, one of the most critical problems in utilization of biomass via gasification and/or pyrolysis at low temperature (500–650 °C) is the formation of tars, an undesirable reaction that is an impediment to the commercialization of the biomass utilization process. These tars, such as benzene, toluene, and naphthalene are largely aromatic hydrocarbons which harness large amounts of energy, thereby lowering the energy content of the product gas. In addition, tars also cause operational problems when cooled and condensed in heat exchangers, lowering heat transfer efficiencies, plugging pipes, and so on. Therefore, efficient conversion of biomass tars is crucial in the biomass gasification and/or pyrolysis processes. Among many processes [6,7], catalytic steam reforming of biomass tar is a considerably attractive approach since it produces syngas which is a high-value gas product [8–10]. Hence, it is essential to develop highly effective catalysts that are capable of converting the biomass tar to synthesis gas with high efficiency. The steam reforming of tars proceeds according to the reactions as shown below and is associated with the water gas shift (WGS) reaction as one of the side reactions [11–13].

$$C_xH_y + xH_2O \rightarrow xCO + (x + y/2)H_2 \text{ (for tars)} \quad (1)$$

$$C_7H_8 + 7H_2O \rightarrow 7CO + 11H_2 \text{ (for toluene S/C = 1)} \quad (2)$$

$$CO + H_2O \rightarrow CO_2 + H_2 \text{ (WGS reaction)} \quad (3)$$

Other reactions such as dry reforming, hydrodealkylation, carbon formation by toluene decomposition and cracking are also included in this process. Furthermore, the effectiveness of sup-

* Corresponding author. Tel.: +65 6516 6312; fax: +65 6779 1936.
E-mail address: chekawis@nus.edu.sg (S. Kawi).

http://dx.doi.org/10.1016/j.apcatb.2015.02.017
0926-3373/© 2015 Elsevier B.V. All rights reserved.

ported metal catalysts for steam reforming of biomass tar has been widely reported [14–20]. In particular, Ni catalysts have been widely investigated for the steam reforming of biomass tar due to its low cost and high activity [16,17]. However, the main drawback for Ni-supported catalysts for use in steam reforming of hydrocarbons is its rapid catalyst deactivation due to the encapsulation of carbon and sintering or loss of active Ni component at high temperature

On the other hand, the layered double hydroxides, anionic clays or hydrotalcite (HT)-like compounds, are a family of materials that have gained much attention in recent years [21–24]. The structure of the HT-like compounds is very similar to that of brucite $Mg(OH)_2$, in which each magnesium cation is octahedrally surrounded by hydroxyls. The HT-like compounds may be represented by the general formula $[M^{2+}{}_{1-x}\ M^{3+}{}_{x}\ (OH)_2]^{x+}\ (A^{n-})^{x/n} \times mH_2O$, where M^{2+} and M^{3+} represents divalent and trivalent cations, respectively and A^{n-} represents interlayer charge-balancing anion. The formation of a HT-like compound greatly depends on molar ratio of $M^{3+}/M^{2+}+M^{3+}$, which may vary from 0.20 to 0.33. In addition, HTs can be easily synthesized by a co-precipitation method, usually at slightly elevated temperature and at a constant pH. Upon high temperature calcinations, the HTs form mixed metal oxides that exhibit several significant properties such as large surface area, basic character, high homogeneity, thermally stable dispersion of metal ion components and synergetic effects are displayed between the elements. Due to these special properties and variable composition, the HT-like compounds are widely used as catalysts, catalyst supports, ion exchangers, molecular sieves and absorbents. In the case of catalytic applications, $MgO–Al_2O_3$-derived HTs have been widely investigated for catalytic reforming of biomass tar [25–27], methane [28] and propane [29], and methane decomposition [30], and etc. Besides the commonly investigated $NiO–MgO–Al_2O_3$ catalysts, $NiO–CaO–Al_2O_3$ catalysts have become more appealing for many researchers in steam reforming of hydrocarbons and alcohols applications in view of its bi-functional characteristic property. Bi-functional implies that the steam reforming performance is associated with Ni species and CaO species which possess the sorption property. This sorption property of CaO plays a crucial role in shifting the equilibrium of steam reforming associated reactions like water-gas-shift reactions toward higher H_2 production rates. The bi-functional application of $NiO–CaO–Al_2O_3$ catalysts for other reactions like steam reforming of methane [31], ethanol [32] and dry reforming of methane [33] has also been reported recently.

Furthermore, in the case of steam reforming of model biomass tar compound, i.e., toluene reactions, with simultaneous catalytic H_2 production and CO_2 capture at 700 °C, it has been reported recently that the dispersed CaO species over olivine catalysts shows higher toluene conversions in terms of H_2 production rates compared to bulk CaO and olivine. $Ni/CaO–Ca_{12}Al_{14}O_{33}$-like catalysts are used for steam reforming of toluene reaction, where CaO is for CO_2 sorption and $Ca_{12}Al_{14}O_{33}$ acts as a support for both CaO and Ni active species [34]. The enhanced production of H_2 via the sorption of CO_2 by CaO species present in the calcined scallop shell during the steam reforming of biomass is also reported elsewhere [35]. In addition to that, sorption enhanced catalytic steam reforming gasification process has also been reported as a direct route from lignocellulosic biomass to high purity hydrogen. Therein, CaO as a sorbent is mixed with HT-derived bi-metallic catalysts has been investigated for steam reforming of chestnut wood sawdust [36]. From the above reported studies on steam reforming of biomass tar reforming process, it can be concluded that well dispersed, supported CaO species are more stable and effective in displaying its sorption property during steam reforming reaction at higher temperature. This sorption property of CaO can be helpful in shifting the equilibrium of WGS reaction toward higher H_2 production rates. Moreover, the synergism between Ni and CaO species can significantly enhance both the reforming activity and sorption property of the catalyst.

By considering the above studies, we aim to synthesize uniformly distributed $NiO–CaO–Al_2O_3$ catalysts and to establish some synergism between NiO and CaO species during the synthesis. Hence, we have opted to synthesize $NiO–CaO–Al_2O_3$ catalysts via HT route in the present work. Various HT-derived $NiO–CaO–Al_2O_3$ catalysts have been successfully synthesized using co-precipitation method and the synthesized $NiO–CaO–Al_2O_3$ HTs were investigated for steam reforming of toluene (SRT, as a biomass tar model compound) and α-cellulose (as a biomass model compound) at 650 °C. The catalytic properties of $NiO–CaO–Al_2O_3$ catalysts for toluene reforming reaction were correlated with sorption properties of the catalysts.

2. Experimental

2.1. Preparation of $NiO–CaO–Al_2O_3$ catalysts

$NiO–CaO–Al_2O_3$ HT-like precursors were prepared by the co-precipitation method [32]. Solution A as the nitrate solution was prepared by dissolving $Ni(NO_3)_2{\cdot}6H_2O$, $Ca(NO_3)_2{\cdot}4H_2O$ and $Al(NO_3)_3{\cdot}9H_2O$ at room temperature, with desirable Ni/Ca/Al molar ratios. The concentration of Ni^{2+} cation was chosen to yield ~10 wt% metal loading in $NiO–CaO–Al_2O_3$ catalysts. Solution B was prepared by dissolving NaOH (1.6 M) and Na_2CO_3 (0.1 M) in deionized water. Then solution A was quickly added to solution B with vigorous stirring. The mixture was heated to 70 °C and held for 2 h. The resultant slurry was filtered and washed with deionized water until a neutral pH was obtained, followed by drying at 100 °C for 24 h in an oven to obtain raw HT-like precursors. The raw precursors were calcined at 800 °C for 5 h for conversion to $NiO–CaO–Al_2O_3$ catalysts. The samples are denoted as Ni–Ca–Al(x:y:z), where x, y and z represents the molar quantities of Ni^{2+}, Ca^{2+} and Al^{3+} elements in the $NiO–CaO–Al_2O_3$ catalysts, respectively. The same preparation method was adopted to prepare NiO–CaO and $NiO–Al_2O_3$ reference catalysts.

2.2. Biomass

α-Cellulose is used as a model compound for biomass material. α-cellulose is obtained from Aldrich chemicals. The dry weight percentage of α-cellulose was C 42 ± 1%, H 7 ± 0.5%, O 50 ± 1% and S 1 ± 0.5%. The elemental analysis was carried out using PerkinElmer 2400 series II CHNS/O system.

2.3. Catalyst characterization

The surface areas of the freshly calcined catalysts and their supports were measured by N_2 physical adsorption at −196 °C in an ASAP 2020 instrument. The specific surface area was calculated by applying the Brunauer–Emmett–Teller (BET) method. The X-ray diffraction (XRD) pattern of each catalyst was measured on a Shimadzu XRD-6000 diffractometer using Cu Kα radiation. The catalyst was placed on an aluminum slide and scanned from 2θ range between 20° to 80° at a ramp rate of 2°/min. The beam voltage and current used were 40 kV and 30 mA, respectively. The actual compositions of all the calcined catalysts were measured using scanning electron microscope coupled to an energy dispersive spectroscopy (SEM–EDX, Jeol, JSM-6701F). The samples were degassed under vacuum condition to remove impurities. Platinum coating (about 10 nm thickness) was carried out at 20 mA for 40 s. Ni particle sizes for reduced catalysts were measured using TEM imaging. The reduced Ni samples were dispersed in ethanol and droplets were introduced on a copper grid.

H_2 Temperature-programmed reduction (TPR) measurements for fresh catalysts were performed on a Thermo Scientific TPDRO 1100 series system equipped with a thermal conductivity detector (TCD). Prior to the TPR measurement, 0.04 g of catalyst was outgassed in He for 1 h at 300 °C to remove any moisture and then cooled to room temperature. Then 5% H_2/N_2 gas was introduced to the catalyst while the temperature of the furnace was increased at a heating rate of 10 °C/min to 1000 °C.

The surface Ni metal content and dispersion was calculated by using N_2O titration method reported elsewhere [37]. Prior to N_2O titration at 70 °C, the sample (W = 50 mg) was reduced at 750 °C for 1 h under H_2 gas, and then cooled to 70 °C in helium gas flow of 30 mL/min. At this temperature, the N_2O decomposition was carried out by introducing several pulses of N_2O gas using 99.99% N_2O with a loop volume of 250 μL. This was followed by TPR with temperatures up to 750 °C performed in the TPDRO 1100 series system. The amount of the oxidized Ni surface atoms by N_2O decomposition was estimated by measuring the H_2 consumed during TPR analysis, in accordance to Eqs. (4) and (5).

$$Ni + N_2O \rightarrow NiO + N_2 \quad (4)$$

$$NiO + H_2 \rightarrow Ni + H_2O \quad (5)$$

Temperature programmed desorption (TPD) of CO_2 profiles were analyzed using the TPDRO 1100 series system. 100 mg of catalyst sample was used in each analysis. Prior to the adsorption of CO_2, the sample was reduced at 750 °C for 1 h under H_2 gas environment. After that the samples were cooled to 50 °C where CO_2 adsorption was carried out for 30 min and the samples were then purged in He gas for 30 min. Desorption of CO_2 took place while heating the sample from room temperature of 30 °C to 1000 °C with a ramp rate of 10 °C/min.

Shimadzu DTG-60 thermogravimetric analyser (TGA) was used to investigate the CO_2 sorption capacity and stability of Ni–Ca–Al catalyst samples. The heating rate was 10 °C/min. About 10 mg of catalyst was used for each experiment. The sample was first kept at 800 °C for 30 min under He gas in order to desorb H_2O and presorbed CO_2 during the synthesis, and then cooled to 650 °C under He gas. Carbonation was conducted at 650 °C (same as the temperature used for performing steam reforming reactions) for 30 min in CO_2 gas, and decarbonation was conducted at 800 °C in He gas. Multiple carbonation–decarbonation cycles were performed and the cycle was repeated 10 times to determine the stability of the samples.

The catalyst surface analysis was performed using X-ray photoelectron spectroscopy (XPS) from a KRATOS AXIS Hsi 165 equipped with Mg–Kα source (1253.6 eV). Prior to the analysis, the catalyst was reduced at 750 °C under H_2 for 1 h which is the same as the reduction condition during reaction. The sample was then mounted on the standard sample stub using double-sided adhesive tapes. All binding energies were referenced to C 1 s hydrocarbon peak at 284.6 eV.

The total amount and nature of deposited carbon on the spent catalysts were measured using thermogravimetric analysis (TGA) and differential thermal analysis (DTA) on a Shimadzu DTG-60 thermogravimetric analyser, respectively. Around 5 mg of spent catalyst was used in each DTA/TGA experiment and heated in air to 900 °C with a heating rate of 10 °C/min.

2.4. Catalyst evaluation

2.4.1. Steam reforming of toluene

Steam reforming of toluene reactions were carried out in a fixed-bed quartz reactor with an inner diameter of 4 mm and a length of 400 mm as reported previously [38]. The catalyst in each test was sandwiched between quartz wool and placed in the middle of the reactor. The operating conditions were as follows: catalyst amount = 0.1 g; toluene amount = 188 μmol (diluted by He gas); S/C ratio = 1; reaction temperature = 650 °C. Prior to the catalytic reaction, the catalyst was reduced in H_2 (30 mL/min) at 750 °C for 1 h and then purged in Helium (120 mL/min) while the temperature was ramped to the desired reaction temperature. Water and toluene were vaporized at 300 °C in a preheater and mixed with He (120 mL/min) gas before entering the main reactor in the vapor state. The reaction products were then passed through a cold trap maintained at a temperature of 5 °C to condense the unreacted toluene and water from the gasification reaction. The non-condensable gas product was analyzed using a gas chromatograph (HP 6890) equipped with a Carboxen column and a thermal conductivity detector. The chromatogram showed peak areas for all of the reacted gases, which were then converted to volume percentages using a calibration curve. The total flow rate of the product gases was measured using a bubble flow meter. The conversion of toluene was expressed in terms of carbon conversion, which was calculated using the following formula:

$$X_{\text{Toluene}}(\%) = \frac{(n_{CO} + n_{CO_2}) \times 100}{(7 \times n_{\text{rin}})} \quad (6)$$

where n is the molar flow rate of each gas.

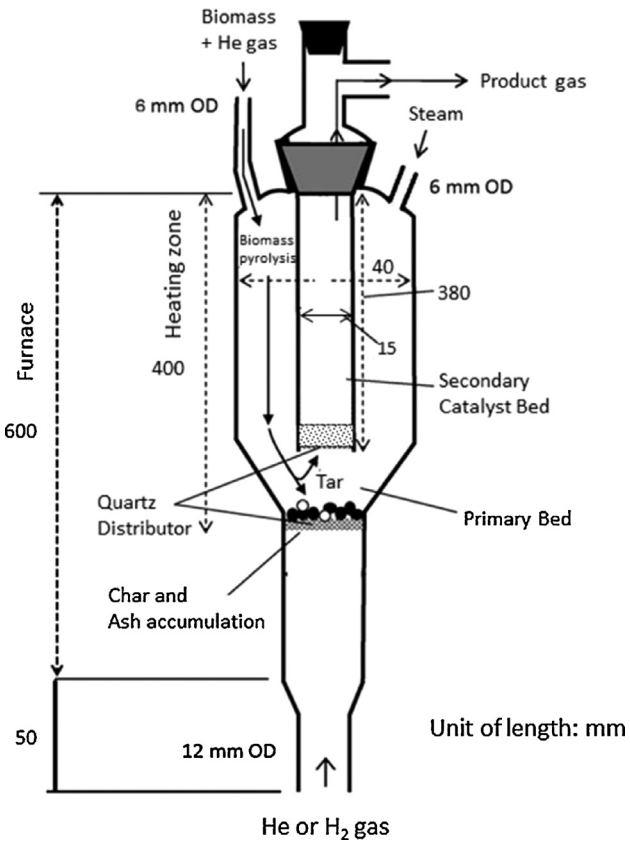

Fig. 1. Schematic diagram of the reactor for catalytic steam gasification of biomass.

2.4.2. Steam reforming of α-cellulose

Steam reforming of α-cellulose as a biomass model compound was carried out in a laboratory-scale continuous feeding dual-bed reactor as illustrated in Fig. 1 based on the reactor design reported in literature [16]. A Nabertherm electric furnace with unit dimension of length = 600 mm and width = 500 mm and having a uniform heating zone of 400 mm is used to control the temperatures of gasification reactor. The reactor displayed in Fig. 1 includes the primary bed for steam gasification of biomass and accumulation of solid products in gasification reaction such as char and ash. The products

in the gas phase at reaction temperatures can include tar as a vapor and they were introduced to the secondary catalyst bed. Tar is liquid at room temperature but at reaction temperature (650 °C), tar can be vaporized and introduced easily to the catalyst bed. The biomass feeder consists of a conical glass vessel with a screw valve at the bottom, allowing continuous feeding of biomass particles by vibrating the glass vessel with an electric vibrator. This feeder is connected on the top of the reactor using a T-joint fitting, which allows simultaneous introduction of biomass particle and carrier gas in to the gasification chamber. Helium was used as a carrier gas to transport the biomass particles into the primary bed. On the top portion of the reactor, there are two more ports; one port for steam feed and another port for the effluent gas. Bottom portion of the reactor has one gas port to introduce He and/or H_2 gas depending on the requirement. Prior to the reforming test, the catalyst (about 0.25 or 0.5 g) was pretreated under H_2 stream of 30 mL/min at 750 °C for 1 h. H_2 gas was introduced from bottom port and no other gases were introduced from the other ports in this pretreatment. During the evaluation of catalytic performance for the steam reforming of biomass, He gas was fed from the bottom of the primary bed reactor through a quartz distributor. At the same time, water was supplied to the reactor using a HPLC pump through one of the top ports. The water is pre heated at 300 °C in order to be introduced into the main reactor in vapor form. The conditions of feeding rate of gases, steam and biomass are described in each figures related to the conversion results. In the steam gasification of biomass, the catalyst fluidization was inhibited by putting few pieces of quartz tubes on the catalyst bed, similar to a fixed bed reactor mode. The reaction temperature was controlled by the thermocouple placed outside the reactor. The catalysts activity tests were carried out under atmospheric pressure. The effluent gas were passed through the filter and a water condenser maintained at 5 °C temperature in order to remove any solid and liquid materials contained in the product gas. The non-condensable gas product was analyzed using a gas chromatograph (HP 6890) equipped with a Carboxen column and a thermal conductivity detector. The total flow rate of the product gases was measured using a bubble flow meter. The carbon-based conversion to gas products was calculated by "A/B × 100", where A represents the formation rate of $CO + CO_2 + CH_4$ and B represents the total carbon supplying rate of biomass. In addition, the yield of carbon-containing gaseous products was also calculated by the ratio of the formation rate to the total carbon supplying rate of biomass. After each experiment, the spent catalyst was collected and measured for the deposited carbon (i.e., coke) over the catalysts using DT/TG analyses. The yield of coke was calculated by (total amount of deposited carbon)/(total carbon amount in fed biomass). Other products, besides gaseous products and coke are considered as Tar + Char, whereby their yield was estimated as (100 – carbon based conversion(%) – coke yield(%)).

3. Results and discussion

3.1. XRD analysis of as-prepared Ni–Ca–Al samples

XRD patterns of as-prepared Ni–Ca–Al HTs with varying $(Ni^{2+} + Ca^{2+})/Al^{3+}$ ratios are presented in Fig. 2. The presence of crystalline hydrotalcite structure is clearly observed in all the XRD patterns. In addition to hydrotalcite structure, all Ni–Ca–Al samples have characteristic peaks of $CaCO_3$ phase, which agrees with the previous studies on the synthesis of Ca–Al and Ni–Ca–Al HTs [39,40]. Using the co-precipitation method to form HTs which consists of Ca^{2+}, the ratio of Ni^{2+}/Al^{3+} utilized was less than the required ratio of 2 to form the HTs structure. The segregation of a $CaCO_3$ phase instead of a pure HTs phase could be attributed to the greater insolubility of $CaCO_3$ and the incompatibility of the ionic sizes of

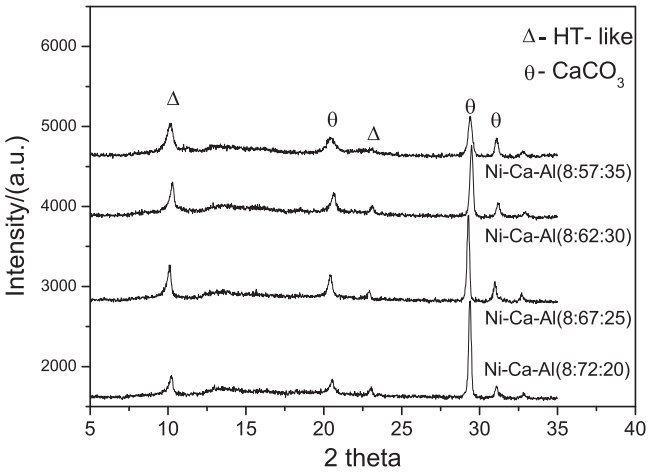

Fig. 2. XRD patterns of as-prepared Ni–Ca–Al HT-like materials with different Ca/Al ratio.

Al and Ca (0.054 nm versus 0.100 nm) [40]. Furthermore, the segregation of this $CaCO_3$ phase was found to increase with increasing amount of Ca^{2+} ions in the samples. On the other hand, the crystallization degree for Ni–Ca–Al(8:72:20) sample was observed to be fairly weak compared to other samples and this could be due to the high molar ratio of $(Ni^{2+} + Ca^{2+})/Al^{3+}$ in this sample. Finally, the formation of hydrotalcite-like and $CaCO_3$ phases for all as-prepared Ni–Ca–Al catalysts were confirmed through XRD analysis

3.2. Time dependent steam reforming of toluene

The catalytic performance for steam reforming of toluene as a biomass tar model compound at low steam-to-carbon ratio of 1 was carried out in a continuous fixed-bed reactor over Ni–Ca(8:92), Ni–Al(8:92) and Ni–Ca–Al catalysts. The time-dependent catalytic performances of Ni–Ca(8:92), Ni–Al(8:92) and Ni–Ca–Al catalysts are depicted in Fig. 3. In Fig. 3, the catalytic performance for all the catalysts are showed up to 24 h reaction time except for Ni–Ca(8:92) (for 5 h, in Fig. 3a) and Ni–Ca–Al(8:72:20) (for 12 h, in Fig. 3b). For these catalysts, the reaction was stopped at shorter reaction times as the reactor was blocked. This could be caused by the deposition of higher amounts carbon species on the catalysts during SRT reaction which resulted the blockage and pressure build-up. In this SRT reaction, the main product stream consists of H_2, CO, CO_2, and trace amounts of CH_4 (<1%). According to Fig. 3, among all the catalysts tested, Ni–Ca–Al(8:62:30) catalyst (in Fig. 3d) shows better catalytic performance of toluene conversion of around 70% and nearly stable activity for 24 h reaction time at S/C of 1. Recently, we have reported [12] that Ni supported on an $Fe_2O_3 - Al_2O_3$ support calcined at 500 °C [NFA(500)] gave a toluene conversion of more than 90% for a period of 26 h with a H_2/CO value of 4.5. However, the S/C value used for NFA(500) catalyst is 3.4 which is comparatively higher for the catalysts studied in the present manuscript which were tested under S/C value of 1. On the other hand, at S/C of 1, NFA(500) gave a toluene conversion of less than 40% with a H_2/CO value of 2. This suggests the performance of Ni–Ca–Al(8:62:30) is promising compared to NFA(500) at especially at the lower S/C reaction conditions, which is less energy consuming. It is also observed that all Ni–Ca–Al catalysts derived from HT-like precursors generally showed better catalytic performance over Ni–Ca(8:92) and Ni–Al(8:92) catalysts. The product distribution in terms of H_2/CO values are in the similar range of 2.5 to 3.0 for all the catalysts. However, this value is generally higher than the H_2/CO value of 1.6 produced from the stoichiometric condition of steam reforming of toluene. The higher

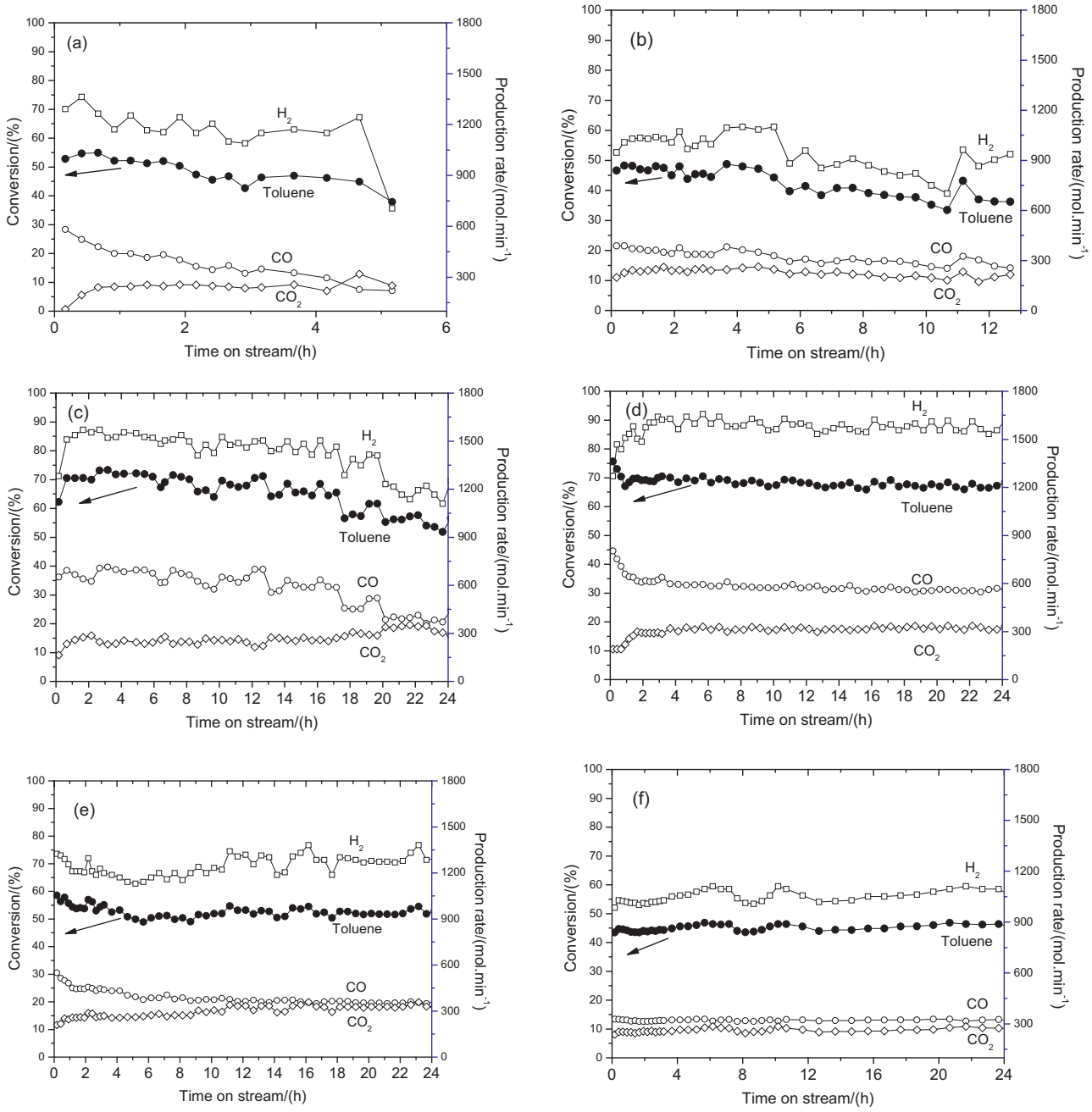

Fig. 3. Steam reforming of toluene performance of (a) Ni–Ca(8:92), (b) Ni–Ca–Al(8:72:20), (c) Ni–Ca–Al(8:67:25), (d) Ni–Ca–Al(8:62:30), (e) Ni–Ca–Al(8:57:35) and (f) Ni–Al(8:92) catalysts. Reaction condition: toluene = 188 μmol min^{-1}; S/C = 1; He = 5357 μmol min^{-1}; W = 100 mg; reaction temperature = 650 °C.

H_2/CO ratio obtained indicates the participation of side reactions to produce more H_2 and/or consume more CO. According to present results and previous reports [13], the SRT reaction is postulated to proceed according to Eq. (2), followed by the WGS reaction (Eq. (3)). This suggests that the SRT performance of any catalyst is also dependent on their ability in promoting the WGS reaction. Furthermore, with reference to literature [12,18,41], it is noted that the performance of Ni-based catalysts in SRT reaction in terms of conversion is majorly dependent on the size and the amount of surface Ni° species available. On the other hand, the long term performance can be influenced by carbon deposition rates on the catalyst, basic characteristics of the catalyst and possible changes in the phase and size of active Ni° centers during SRT reaction. In this article, DT/TG experiments were carried out to understand the nature and rate of carbon deposited over all the catalysts during SRT reaction. It was found that Ni–Ca–Al(8:62:30) catalyst has lower carbon deposition rates compared to others, and the detailed analysis will be discussed latter. XRD patterns of reduced and spent catalysts showed that the Ni° agglomeration is considerable lower for Ni–Ca–Al(8:62:30) catalyst compared to all other higher CaO-containing Ni–Ca–Al catalysts. The lower catalytic performance of Ni–Ca–Al(8:57:35) compared to the other Ni–Ca–Al catalysts could be due to availability of lower amounts of surface Ni species and basicity of the catalyst.

The initial performances shown in Fig. 3 are further interpreted in order to understand the influence of sorption property of the catalysts on the performance of steam reforming of toluene reaction in terms of H_2 production rates and CO_2 selectivity. The time dependent H_2 production rates and CO_2 adsorption behavior for Ni-Ca(8:92), Ni-Al(8:92) and Ni–Ca–Al catalysts during SRT reaction

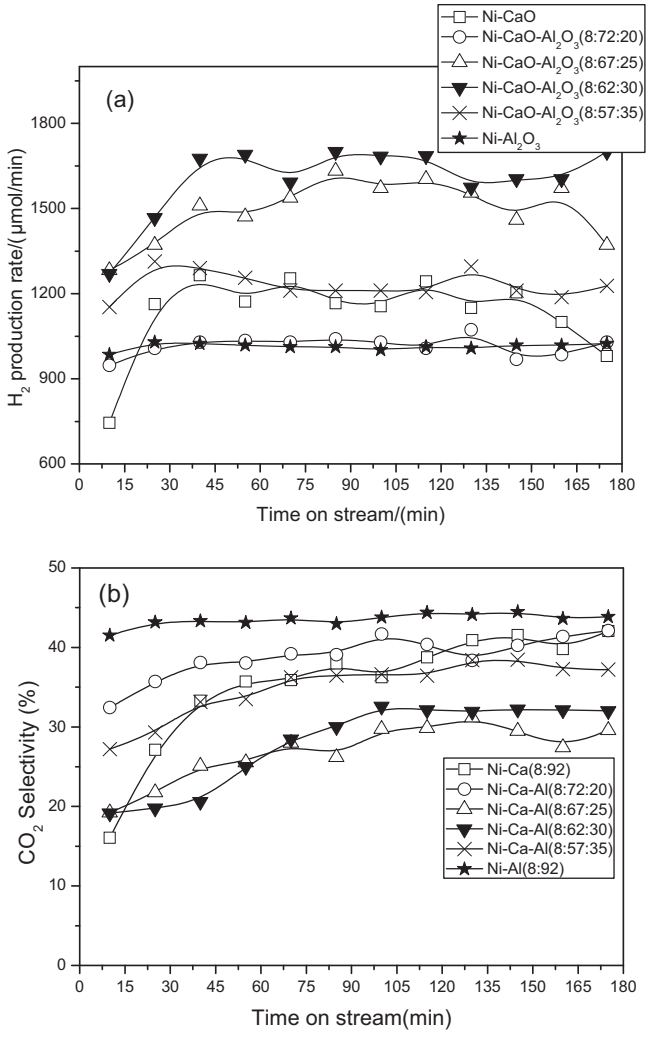

Fig. 4. Initial catalytic behavior in terms of (a) H_2 production rate and (b) CO_2 selectivity for steam reforming of toluene reaction. Reaction condition: toluene = 188 μmol min^{-1}; S/C = 1; He = 5357 μmol min^{-1}; W = 100 mg; reaction temperature = 650 °C.

for the initial 3 h of reaction are presented in Fig. 4. In Fig. 4a, The H_2 production rates for Ni–Al_2O_3 is lower and more stable throughout the reaction time of 3 h compared to other catalysts. In this case, the H_2 production rate is dependent on steam reforming activity because the Ni/Al(8:92) catalyst does not possess CO_2 sorption capacity. On the other hand, the H_2 production rates for Ni–Ca(8:92) and Ni–Ca–Al catalysts are stable only after nearly 45 min of reaction time. In this case, the H_2 production rate depends on steam reforming activity and also on the CO_2 sorption capacity of the catalysts. As reported in the literature [34], the latter phenomenon may lead to a shift of water gas shift reaction toward increased H_2 production and simultaneous increase in CO_2 production (Le Chatelier principle). From Fig. 4, it can also be observed that the catalysts Ni–Ca–Al (8:62:30) and Ni–Ca–Al (8:67:25) have higher H_2 production rates and also lower CO_2 selectivity. This behavior demonstrates their good catalytic activity and the effect of CO_2 sorption on the WGS reaction equilibrium. Similar behavior is also reported over CaO/olivine catalysts for SRT reaction at 700 °C [34]. The CO_2 adsorption behavior of olivine supported by CaO catalysts showed higher H_2 production rates and lower CO_2 selectivity compared to olivine alone as a steam reforming catalyst. It can also be observed from Fig. 4b that the CO_2 selectivity for all CaO containing catalysts is generally lower than that of Ni/Al(8:92) catalyst. This result suggests that the presence of CaO species in Ni–Ca–Al can enhance the CO_2 sorption capacity of the catalysts directly implying an enhancement of H_2 production rate during SRT reaction at 650 °C. Finally, it can also be concluded that a synergy between the Ni species and CaO species of Ni–Ca–Al catalysts as in Ca(Ni, Al)O solid solution results in bi-functional property of Ni–Ca–Al catalyst which in turn leads to promising performance in steam reforming of tar reaction.

3.3. Steam reforming of α-cellulose

In order to further validate the catalytic behavior of Ni–Al(8:92), Ni–Ca(8:92) and Ni–Ca–Al catalysts, these catalysts were then tested in steam reforming of α-cellulose. The α-cellulose is chosen as a model compound of biomass because α-cellulose is reported as one of the major component found in many biomass materials [42–44]. Fig. 5 shows, catalytic performance of Ni–Ca(8:92), Ni–Al(8:92) and Ni–Ca–Al catalysts in the steam reforming of α-cellulose together with steam gasification of α-cellulose without catalyst at 650 °C. The results presented in Fig. 5 are based on the average performance of the catalysts for an initial 30 min of reaction time. Without catalyst, the carbon based yield from the formation of CO was lesser compared to that with Ni-based catalysts. The formation rate of hydrogen was also much lower than on the Ni-based catalyst and with a H_2 to CO (H_2/CO) value of 0.27. Another important point to highlight is that the yields of char + tar were higher without any presence of catalysts. According to Fig. 5, it is also found that all Ni-based catalysts not only significantly decreased the carbon based yields of char + tar but they also enhanced the formation rate of hydrogen. This suggests the importance of catalysts in enhancing the H_2 production rate as well as reducing the amount of tar residues. Among all the catalysts tested, it is observed that Ni–Ca–Al(8:62:30) catalyst showed higher H_2 production rates (1989 μmol min^{-1}) and lower carbon based yields of char + tar (14.6%). On the other hand, almost all the catalysts showed deposition of coke during the reaction. The amount of coke deposited is also reported in Fig. 5. The amount of carbon deposited in Fig. 5 was in the range between 0.8 and 4 wt% carbon/g-cat.

3.4. Catalyst stability study for steam reforming of cellulose

The performances of Ni–Ca–Al(8:62:30) and Ni-Al(8:92) catalysts were further compared in terms of stability with longer reaction times. Fig. 6 shows the changes of formation rates of H_2, CO, CO_2 and CH_4 with reaction time at 650 °C. Fig. 6a shows the Ni–Ca–Al(8:62:30) catalyst exhibiting stable formation rates of H_2, CO at all reaction times having a H_2/CO value of around 1.0. The formation rate for CO_2 is decreased while the formation rate of CH_4 increased slightly after 60 min reaction times. On the other hand, for Ni/Al_2O_3 catalysts, the formation rates of CO, H_2 and CO_2 gases decreased with CH_4 increasing as the reaction proceeds. This phenomenon might be related to the catalyst deactivation [25]. It is also observed that the formation rates of H_2 and CO_2 gases are significantly higher for Ni–Ca–Al(8:62:30) catalysts than Ni–Al(8:92) at all reaction times. Thus, these results indicate that Ni–Ca–Al(8:62:30) catalyst prepared from hydrotalcite precursors is much more active and stable than Al_2O_3 supported Ni catalysts.

3.5. Thermo-gravimetric analysis for sorption capacity at 650 °C

Thermo-gravimetric analysis was carried out to evaluate the sorption capacities and stabilities of Ni–Ca–Al catalysts. Fig. 7 displays the sorption capacities of Ni–Ca–Al catalysts against sorption cycles. It shows that the CO_2 sorption capacity has a positive correlation with CaO content in the catalysts, since CaO is an active chemosorbent for CO_2 [40]. The Ni–Ca–Al (8:72:20) catalyst shows

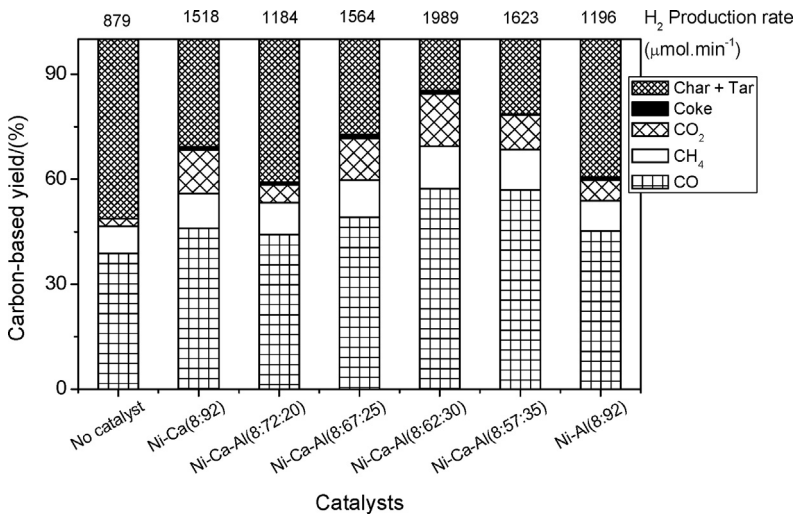

Fig. 5. Catalytic performance of Ni–Ca(8:92), Ni–Ca–Al and Ni–Al(8:92) catalysts in steam reforming of biomass. Reaction condition: W = 250 mg; α-cellulose = 150 mg min^{-1}; He = 90 mL min^{-1}; S/C = 0.5; reaction temperature = 650 °C; reaction time = 30 min; reduction temperature = 750 °C/1 h.

a maximum CO_2 sorption value of 23.8% in the first cycle which is higher than the other catalysts. It is widely accepted that carbonation of CaO proceeds via two stages; a rapid heterogeneous chemical reaction and a diffusion controlled reaction caused by the formation of a $CaCO_3$ layer [45,46]. The sorption ability depicted in Fig. 7 is decreased slightly with each cycle, showing that the CaO in the catalysts can react with CO_2 to form $CaCO_3$, but not all the $CaCO_3$ formed in the process could reversibly transform to CaO. This could be due to the sintering of CaO and the change of physical properties during multiple carbonation and decarbonation cycles [45,47]. This decrease in the sorption ability is calculated to be 9, 18, 5 and 20% over Ni–Ca–Al(8:57:35), Ni–Ca–Al(8:72:20), Ca–Al(8:62:30) and Ni–Ca–Al(8:67:25) catalysts, respectively. The stability in sorption capacity can be related to its physical properties such as the smaller CaO crystallite size and larger pore volume as shown in Table 1 [39,40]. By comparing the sorption capacities, it can be concluded that an appropriate Ca/Al ratio in Ni–Ca–Al catalysts plays a key role in the formation of a well-distributed space structure containing Ni, CaO and Al_2O_3 species. This well-distribution retards the sintering of CaO micrograins during calcination and therefore contributes significantly to the CO_2 sorption capacity and stability.

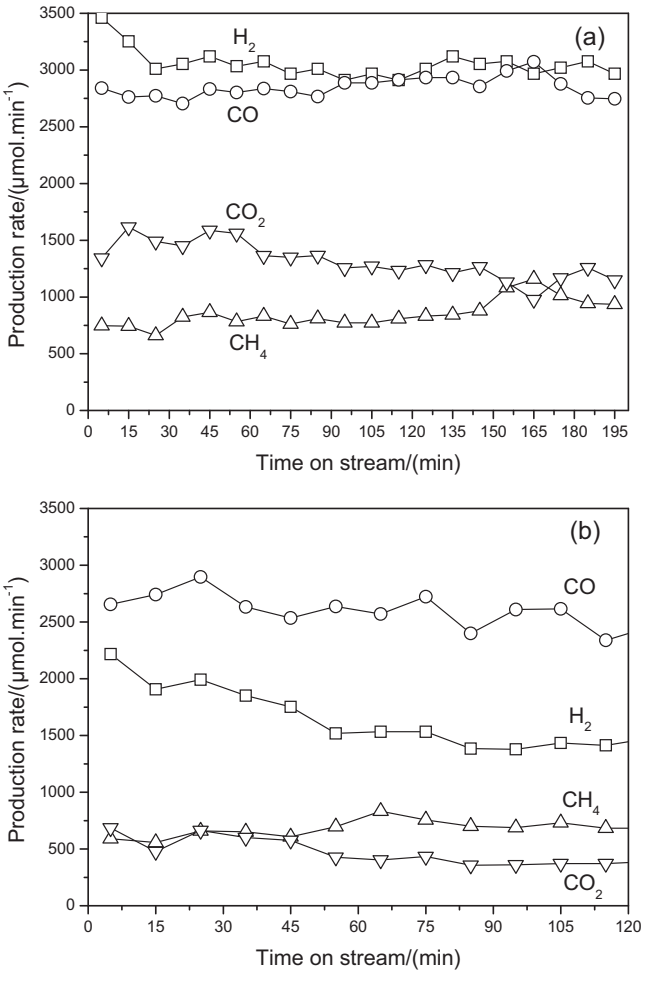

Fig. 6. Changes of catalytic performances in steam reforming of biomass with time on stream over (a) Ni–Ca–Al(8:62:30) and (b) Ni–Al(8:92) catalysts. Reaction condition: W = 500 mg; α-cellulose = 150 mg min^{-1}; He = 90 mL min^{-1}; S/C = 0.5; reaction temperature = 650 °C; reaction time = 30 min; reduction temperature = 750 °C/1 h.

3.6. Physicochemical properties of the catalysts

Physicochemical properties, i.e., BET surface area and actual elemental compositions for fresh catalysts are presented in

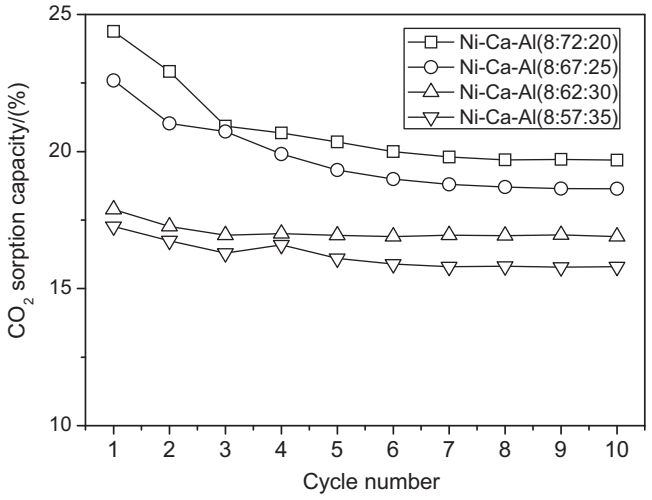

Fig. 7. Comparison of cyclic sorption capacity of Ni–Ca–Al catalysts. Condition: carbonation temperature = 650 °C; De-carbonation temperature = 800 °C.

Table 1
Physical properties of freshly calcined catalysts.

Catalyst	[a]Actual compositions (Ni:Ca:Al)	BET-SA ($m^2\ g^{-1}$)	Crystallite size of NiO (nm)	Crystallite size of CaO (nm)	Pore volume ($cm^3\ g^{-1}$)	Average pore size (nm)
Ni–Ca(8:92)	11.7:88.3:–	42	25.4	30.9	0.109	10.33
Ni–Ca–Al(8:72:20)	12.1:65.7:22.3	18	7.2	13.3	0.085	22.15
Ni–Ca–Al(8:67:25)	12.8:60.1:27.1	15	8.2	13	0.096	26.06
Ni–Ca–Al(8:62:30)	12.4:57.1:30.5	12	8.4	13.5	0.114	38.97
Ni–Ca–Al(8:57:35)	12.1:55.7:32.3	20	5.4	13.3	0.183	37.39
Ni–Al(8:92)	21.6:–:78.4	159	n.d.	–	0.358	8.98

[a] Determined from SEM–EDX for calcined catalysts.

Table 2
H_2 uptakes, dispersion, Ni° particle and crystallite size values for the catalysts.

Catalyst	[a]H_2 uptakes ($\mu mol\ g-1$)	D (%)	Particle size of Ni° (nm)		[c]Crystallite size of Ni°(nm)	
			[a]N_2O	[b]TEM	Reduced	Spent
Ni–CaO(8:92)	125.3	6.5	14.9	20–40	18.4	24.4
Ni–Ca–Al(8:72:20)	221.7	10.8	8.9	7–15	8.1	23.7
Ni–Ca–Al(8:67:25)	168.7	8.1	11.9	7–15	8.7	21.3
Ni–Ca–Al(8:62:30)	154.6	7.2	13.4	7–15	8.8	12.1
Ni–Ca–Al(8:57:35)	107.9	4.9	19.8	7–15	8.8	11.9
Ni–Al(8:92)	401.7	14.8	6.6	5–10	7.8	10.5

[a] Obtained from N_2O chemisorption method [37].
[b] Measured from TEM images of reduced catalysts.
[c] Calculated for reduced and spent catalysts from XRD analysis.

Table 1, whereas the Ni dispersion, particles and crystallites sizes for reduced catalysts and Ni crystallites sizes for spent catalysts are presented in Table 2. It can be seen that the BET surface areas for fresh catalysts are in the order of Ni–Al(8:92) > Ni–Ca(8:92) > Ni–Ca–Al catalysts. The H_2 uptake values presented in Table 2 are obtained from N_2O decomposition experiments according to Eqs. (4) and (5). Next, the Ni dispersion values were calculated by considering H_2:Ni = 1. The Ni particles sizes for reduced catalysts were measured using two methods; firstly using Ni dispersion values obtained from N_2O decomposition method and secondly using TEM images of reduced catalysts. The values obtained from both of these methods are presented in Table 2. It is clear from Table 2 that with the exception of Ni–Ca–Al(8:57:35) catalyst, the Ni particle sizes obtained from N_2O pulse method are within the range of the Ni particle sizes obtained from TEM images i.e., Ni–Al(8:92) > Ni–Ca–Al > Ni–Ca(8:92) catalysts. Furthermore, it is also observed that with the exception of Ni–Ca–Al(8:57:35), the H_2 uptake values and the Ni dispersion (%) derived from N_2O method are also in the order of Ni–Al(8:92) > Ni–Ca–Al > Ni–Ca(8:92) catalysts, which is in good correlation with the Ni particle and crystallite sizes of the reduced catalysts. The Ni dispersion for Ni–Al catalyst is found to be much higher than Ni–Ca(8:92) and Ni–Ca–Al. This might be because of its high surface area as compared to other catalysts. As in the case of reduced Ni–Ca(8:92) catalyst, the Ni dispersion is lower and Ni crystallite size is higher (18.4 nm) than other catalysts, whereby big Ni particles can lead to the deposition of higher amounts of carbon species during SRT reaction. Lower catalytic performance (as in Fig. 3) for Ni–Ca–Al(8:72:20) and Ni–Ca–Al(8:67:25) catalysts compared to Ni–Ca–Al(8:62:30) is related to the bigger Ni crystallites sizes of those catalysts in their spent forms compared to Ni–Ca–Al(8:62:30) catalyst. Furthermore, according to previous reports [18], the steam reforming activity of Ni catalysts can be influenced by the crystallites size and dispersion of Ni species as well as the number of basic sites present in the catalysts. The higher catalytic activity of Ni–Ca–Al(8:62:30) catalysts compared to Ni–Al(8:92) catalyst despite having a higher dispersion and lower Ni crystallite size in the latter case, can be explained based on the strength and amount of available basic centers on those catalysts.

3.7. XRD of calcined, reduced and spent catalysts

The XRD patterns of freshly calcined Ni–Al(8:92), Ni–Ca(8:92) and Ni–Ca–Al catalysts are depicted in Fig. 8A. The patterns in Fig. 8A of Ni–Ca(8:92) and Ni–Ca–Al mainly shows a diffraction peak corresponding to the presence of NiO phase that is centered at around $2\theta = 43.2°$ (JCPDS #01-1239) and CaO phase. The XRD pattern of Ni–Al(8:92) catalyst has reflections corresponding to Al_2O_3 phase while they are nearly invisible for all the Ca-containing Ni–Ca–Al catalysts. This could be either due to the amorphous nature of alumina or the well mixing of this alumina phase with the CaO metal oxide species. The average crystallite size of NiO and CaO were determined and presented in Table 1. It is observed that the NiO crystallite size of 30.9 nm for Ni–Ca(8:92) were estimated to be significantly higher compared to all other catalysts (5.4 nm to 8.4 nm, in Table 1). It is also observed that the average NiO and CaO crystallite sizes of all Ni–Ca–Al catalysts were found to be lower than Ni–Ca(8:92) catalyst even though they have lower surface area value compared to Ni–Ca(8:92) catalyst. Furthermore, Fig. 8B shows the XRD patterns of freshly reduced Ni–Al(8:92), Ni–Ca(8:92) and Ni–Ca–Al catalysts. All of the patterns in Fig. 8B shows a diffraction peak corresponding to the Ni metal phase that is centered at around $2\theta = 44.6°$ (JCPDS #04-0850) and CaO phase for all CaO containing catalysts. The XRD pattern of Ni–Al(8:92) catalyst has reflections corresponding to Al_2O_3 phase while they are nearly invisible for all the Ni–Ca–Al catalysts. The average crystallite size of metallic Ni was determined by broadening of the (1 1 1) line of nickel at around 44.6° [48]. The Ni crystallite sizes were estimated to be significantly higher for Ni–Ca(8:92) (18.4 nm) catalyst compared to all other catalysts (8.0 nm to 8.8 nm, in Table 2). It is also observed that the average Ni crystallite sizes of all Ni–Ca–Al catalysts were found to be lower than Ni–Ca(8:92) catalyst even though they have lower surface area value compared to Ni–Ca(8:92) catalyst. This lower Ni crystallite size of Ni–Ca–Al catalysts is primarily attributed to the fact that these catalysts are derived from HT-like precursors. In the catalysts derived from HT-like precursors, all the metal oxide species were uniformly distributed within the catalysts as a result the Ni species can well be distributed by/with other species like CaO and Al_2O_3 in the catalysts that ultimately restrict the rate of the agglomeration of Ni species during reductive pretreatment at high

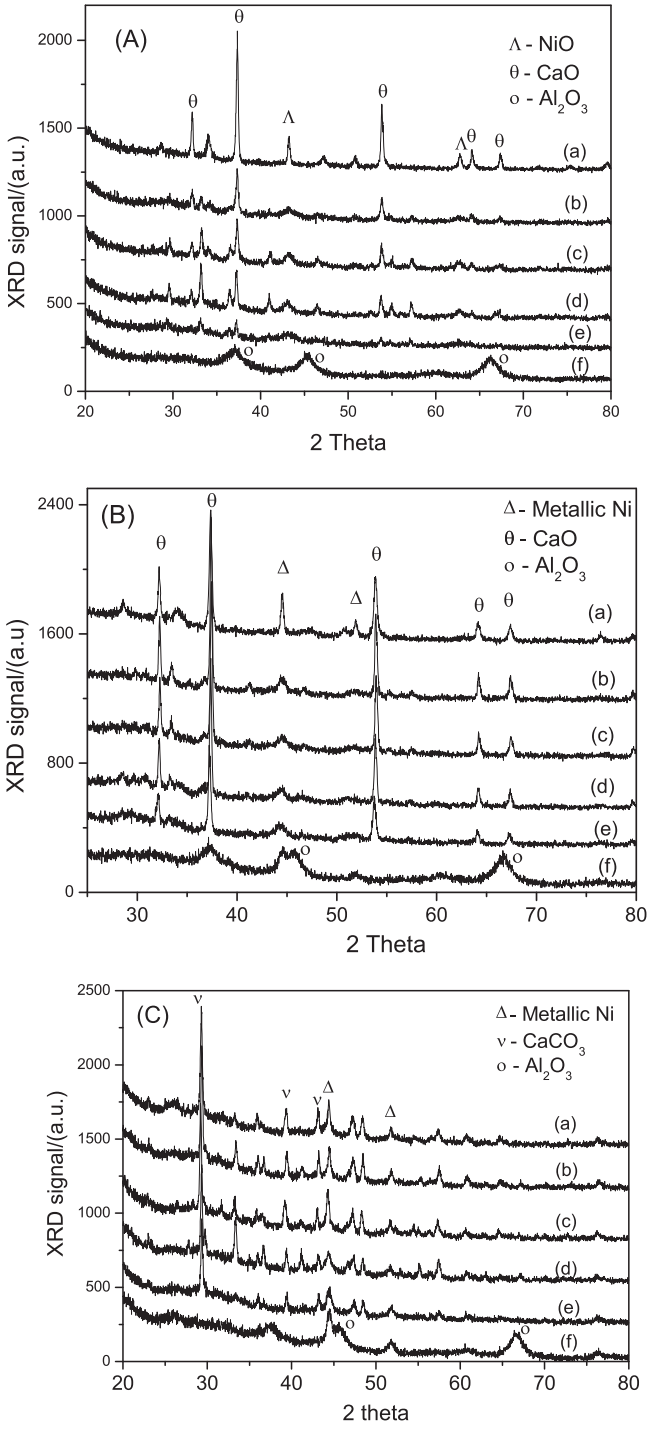

Fig. 8. XRD patterns of (A) freshly calcined, (B) reduced and (C) spent (a) Ni–Ca(8:92), (b) Ni–Ca–Al(8:72:20), (c) Ni–Ca–Al(8:67:25), (d) Ni–Ca–Al(8:62:30), (e) Ni–Ca–Al(8:57:35) and (f) Ni–Al(8:92) catalysts.

temperature [31,32]. The CaO phase present in all CaO containing catalysts is from the decomposition of $CaCO_3$ species formed during the catalysts synthesis and the collapse of HT-like phase during calcination of the catalyst at 800 °C for 5 h in air environment. It is also observed that the intensity of peaks correspond to CaO phase are directly related to the amount of CaO present in the catalysts.

Next, XRD patterns of spent Ni–Al(8:92), Ni–Ca(8:92) and Ni–Ca–Al catalysts collected after the SRT reaction (activity as in Fig. 3) are depicted in Fig. 8C. In Fig. 8C, all the patterns shows the diffraction peaks corresponding to the Ni metal phase (JCPDS #04-0850) and all Ni–Ca–Al catalysts have the reflections corresponding to $CaCO_3$ phase. This $CaCO_3$ phase is formed by carbonation of CaO species present in reduced catalysts during SRT reaction at 650 °C. Similar to Fig. 8A & B, Fig. 8C shows the reflections corresponding to Al_2O_3 phase which is present only in Ni–Al(8:92) catalyst. The average crystallite size of metallic Ni was determined by broadening of the (1 1 1) line of nickel at around 44.6° [48]. The Ni crystallite sizes were estimated to be 24.4, 23.7, 21.3, 12.1, 11.9 and 10.5 nm for Ni–Ca(8:92), Ni–Ca–Al(8:72:20), Ni–Ca–Al(8:67:25), Ni–Ca–Al(8:62:30), Ni–Ca–Al(8:57:35) and Ni–Al(8:92) catalysts, respectively (Table 2). By comparing Ni metallic sizes of reduced and spent catalysts, it is observed that the increase in Ni metallic size is higher for the catalysts having higher amounts of CaO species. Thus, the lower catalytic performance of Ni–Ca(8:92) and Ni–Ca–Al(8:72:20) and Ni–Ca–Al(8:67:25) catalysts over Ni–Ca–Al(8:62:30) catalyst can be explained based on the significant increase in the Ni metallic size due to agglomeration during SRT reaction at 650 °C. From XRD patterns in Fig. 8, it can be concluded that the slow rate of increase in Ni metallic size for Ni–Ca–Al(8:62:30) catalyst during SRT reaction at 650 °C could be one of the reasons for showing superior catalytic performance over other catalysts.

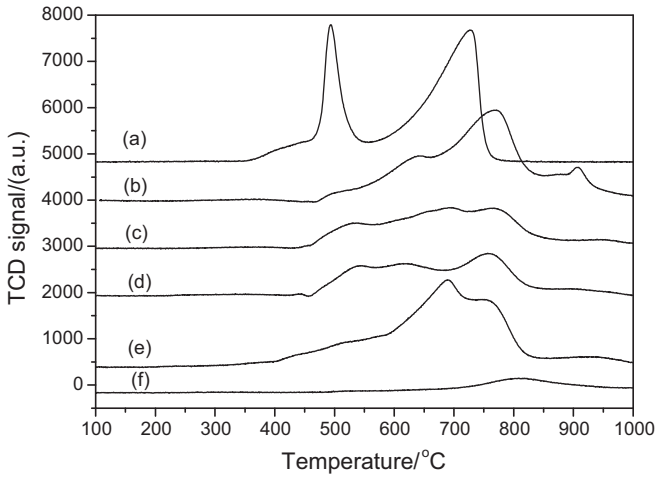

Fig. 9. H_2-TPR profiles of calcined (a) Ni–Ca(8:92), (b) Ni–Ca–Al(8:72:20), (c) Ni–Ca–Al(8:67:25), (d) Ni–Ca–Al(8:62:30), (e) Ni–Ca–Al(8:57:35) and (f) Ni–Al(8:92) catalysts.

3.8. H_2– temperature programmed reduction analysis

The reducibility of the calcined Ni–Al(8:92), Ni–Ca(8:92) and Ni–Ca–Al catalysts were investigated by H_2-TPR experiments, and the obtained profiles are shown in Fig. 9. The H_2-TPR profile of Ni–Ca(8:92) catalyst has two reduction centers. The peaks at about 480 °C and 700 °C are ascribed to the conversion of bulk phase NiO and nickel oxides with interaction with CaO species to Ni°, respectively [49,50]. The H_2-TPR profile of Ni–Al(8:92) catalyst has a single broad high temperature reduction peak centered at around 800 °C which is attributed to the reduction of nickel oxides interacting with Al_2O_3 species to Ni°. The H_2-TPR profiles of Ni–Ca–Al catalysts in Fig. 9 distinguished the presence of three types of Ni species. The first two reduction centers at about 520 °C and 650 °C are ascribed to conversion of bulk NiO and mildly interacting NiO with CaO species to Ni°, respectively. These two reduction centers are also observed in H_2-TPR profile of Ni–Ca(8:92) catalyst. It is also observed that in H_2-TPR profile of Ni–Ca–Al (8:62:30) catalyst, the latter peak is located at slightly lower temperature than other Ni–Ca–Al catalysts. On the other hand, the third high temperature reduction peak centered at about 780 °C is ascribed to the

reduction of nickel oxides which interacted with Al_2O_3 species. This high temperature reduction peak is also present in H_2-TPR profile of Ni–Al(8:92) catalyst. In Fig. 9, the intensities at each peak appear to be different for all Ni–Ca–Al catalysts though all have the same amount of nominal Ni content. This is due to the presence of different amounts of CaO and Al_2O_3 species in Ni–Ca–Al catalysts. It is also observed for Ni–Ca–Al catalysts that the low temperature reduction peak is shifted slightly toward higher temperature region than in Ni–Ca(8:92) catalyst. The moderate and higher temperature reduction peaks are shifted slightly toward lower temperature regions than in Ni–Ca(8:92) and Ni–Al(8:92) catalysts, respectively. This behavior suggests that the Ni^{2+} species in Ni–Ca–Al catalysts are in Ca(Ni, Al)O solid solution, which could be formed from the collapse of HT-like (showed in Fig. 2) structured material during calcination at 800 °C. Similar behavior was also reported for Mg(Ni, Al)O solid solution [25]. It was interpreted that the presence of Al^{3+} in Mg(Ni, Al)O solid solution suppresses the crystallite growth, thus more reducing agents are accessible to the oxide. Based on the TPR results, the reduction temperature of 750 °C is necessary for Ni–Ca–Al catalysts since the active species of steam reforming reaction is Ni metal.

3.9. Temperature-programmed desorption of CO_2

CO_2– TPD analysis was carried out to determine the surface basicity of reduced Ni–Ca(8:92), Ni–Al(8:92) and Ni–Ca–Al catalysts. It is commonly believed that the CO_2 adsorbed on weaker basic sites would be desorbed at lower temperatures, and those adsorbed on stronger basic sites would be desorbed at higher temperatures [51]. The CO_2– TPD profiles of all the catalysts are compared in detail in Fig. 10 up to 700 °C. According to Fig. 10, all Ni–Ca–Al catalysts have three CO_2– desorption peaks. The lower temperature CO_2– desorption peak located in the range of 140–260 °C is assigned to the low-strength basic sites such as bicarbonates, which results from the interaction between CO_2 and the weak basic surface hydroxyl groups. This peak is almost negligible in Ni–Ca(8:92) catalyst but it is the only peak present in Ni–Al(8:92) catalyst. This suggests that this low temperature desorption peak corresponds to the basic centers created by Al_2O_3 species presented in the catalysts. It is also clearly observed that this CO_2– desorption peak was shifted to higher temperature region in Ni–Ca–Al catalysts compared to Ni–Al(8:92) catalyst. This shift to higher temperature region is relatively significant for Ni–Ca–Al(8:62:30) catalyst as the increase is about 120 °C (from 140 °C to 260 °C). This also suggests incorporation of Al^{3+} species into Ni–Ca(8:92) catalyst strengthens the basicity of the catalyst up to an optimum Ni–Ca–Al(8:62:30) catalyst composition. From this, we can propose that in lower temperature region, the basic centers present in Ni–Ca–Al(8:62:30) catalyst are higher in quantity and stronger in strength than other catalysts. However, the desorption peaks located in the narrow range of 365–385 °C might be related to the basic sites with moderate intensities and strengths. The narrow range of CO_2– desorption temperature may suggests that the basic strength of all CaO containing catalysts is similar for this region. Lastly, the peak ranging from 585–660 °C is probably due to high-strength basic sites such as uni-dentate carbonates. According to literature, this high temperature CO_2– TPD peak is generally observed in higher CaO loaded catalysts which could be due to the oversaturation of Ca species that exist as a separate CaO phase, and have stronger adsorption strength of CO_2 compared to Ca ions dispersed in the Al_2O_3 matrix. Furthermore, the basicity of all the catalysts in terms of amount of CO_2 desorbed has been determined from the area under the CO_2 desorption profiles presented in Fig. 10. The amount of basicity were obtained to be 2443.1, 237.8, 385.7, 686.6, 328.2 and 380.9 μmol g^{-1} for Ni–Ca(8:92), Ni–Ca–Al(8:72:20), Ni–Ca–Al(8:67:25), Ni–Ca–Al(8:62:30), Ni–Ca–Al(8:57:35) and Ni–Al(8:92) catalysts, respectively. It is observed that with the exception of Ni–Ca(8:92) catalyst, the amount of CO_2 desorbed is higher for Ni–Ca–Al(8:62:30) catalyst compared to all other catalysts. On the other hand, Fig. S2 shows the correlation between the amount of basicity and carbon deposition rates during SRT reaction at 650 °C against the catalysts. Overall, it can be concluded that the basic strength in Ni–Ca–Al catalysts is significantly enhanced at lower temperature region while it is almost similar to the Ni–Al(8:92) and Ni–Ca(8:92) catalysts at higher temperature regions. This extra basicity on Ni–Ca–Al catalysts enables them to neutralize the acidity of the supports effectively, thereby suppressing cracking and polymerization reactions. This suppression in turn leads to enhanced steam-coke reaction, which ultimately decreases the carbon deposition over active metal surface during SRT reaction.

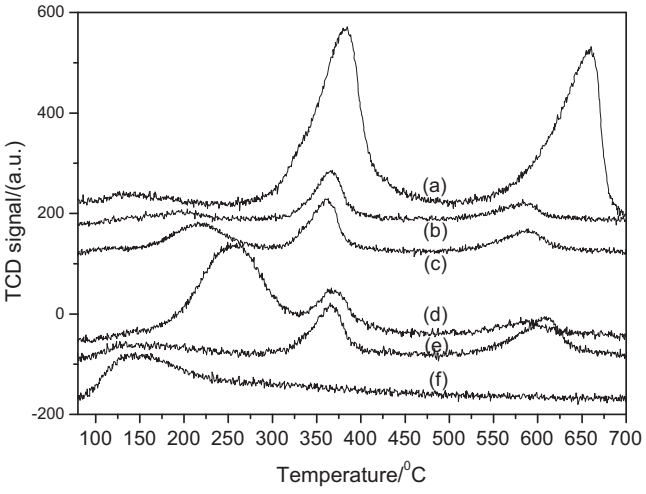

Fig. 10. TPD-CO_2 profiles of reduced (a) Ni–Ca(8:92), (b) Ni–Ca–Al(8:72:20), (c) Ni–Ca–Al(8:67:25), (d) Ni–Ca–Al(8:62:30), (e) Ni–Ca–Al(8:57:35) and (f) Ni–Al(8:92) catalysts.

3.10. XPS analysis

A comparative XPS study was done in order to understand the surface species present in the freshly reduced Ni–Al(8:92), Ni–Ca–Al and spent Ni–Ca–Al(8:62:30) catalysts. Fig. 11a displays the binding energies (BEs) of Ni $2p_{3/2}$ species present in reduced Ni–Al(8:92) and Ni–Ca–Al catalysts. There are two kinds of Ni 2p BEs, firstly due to the presence of Ni^0 (~852.4 eV) species and secondly due to the presence of Ni^{2+} (~855.2 eV) species, where the Ni^{2+} species interacts with Al and/or Ca species present in Ni–Al and Ni–Ca–Al catalysts [52]. In Fig. 11a for Ni–Ca–Al catalysts, proceeding from Ni–Ca–Al(8:72:20) to Ni–Ca–Al(8:57:35), both the BE values of Ni 2p are shifted slightly to higher values. This shift is very obvious for Ni–Al(8:92) catalyst when compared with Ni–Ca–Al catalysts, indicating that the Ni species present in Ni–Ca–Al catalysts have weaker interactions with Al species as compared with those in the Ni–Al(8:92) catalyst. This result suggests that the Ni–Ca–Al catalysts might be in Ca(Ni, Al)O solid solution form, affirming the observations in the TPR profiles presented in Fig. 9. Next, the Ni 2p BEs of spent (after 23 h reaction time in SRT reaction) together with the reduced Ni–Ca–Al(8:62:30) catalyst are displayed in Fig. 11b. It is evident that there also exists two kinds of Ni species, namely, Ni^0 (BE at 852.8 eV) and Ni^{2+} (BE at 855.5 eV) in the spent catalyst. However, the Ni 2p BEs of spent catalyst was shifted slightly to higher values compared with the Ni 2p BE values observed in reduced catalyst. This shift to higher BE values in spent Ni–Ca–Al(8:62:30) catalyst indicates that the

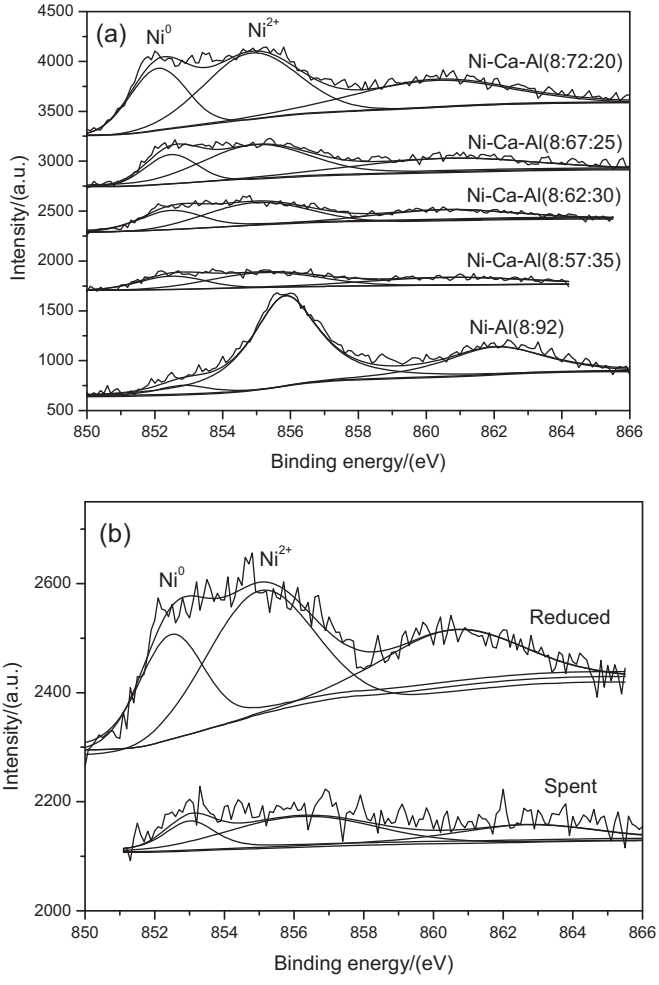

Fig. 11. Ni 2p binding energies of (a) freshly reduced and (b) spent Ni–Ca–Al(8:62:30) catalysts.

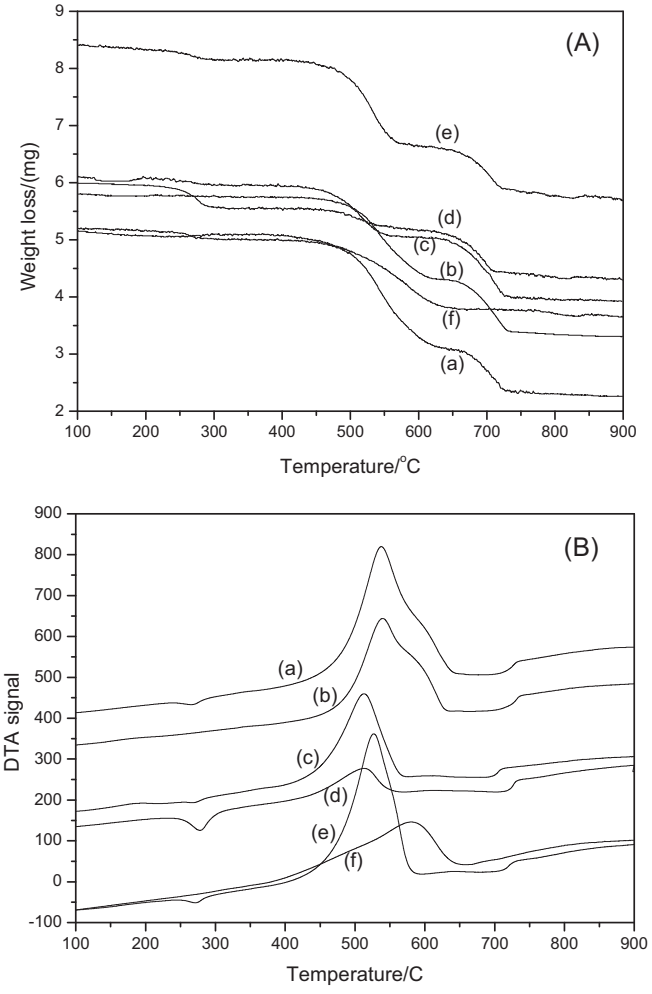

Fig. 12. The TGA (A), DTA (B) profiles of spent (a) Ni–Ca(8:92), (b) Ni–Ca–Al(8:72:20), (c) Ni–Ca–Al(8:67:25), (d) Ni–Ca–Al(8:62:30), (e) Ni–Ca–Al(8:57:35) and (f) Ni–Al(8:92) catalysts. Reaction condition: toluene = 188 μmol min^{-1}; S/C = 1; He = 5357 μmol min^{-1}; W = 100 mg; reaction temperature = 650 °C.

Table 3
Surface composition of elements present in reduced Ni–Al(8:92) and Ni–Ca–Al, and spent Ni–Ca–Al(8:62:30) catalysts.

Catalyst	[b]Surface molar composition (%)			
	Ni	Ca	Al	O
Ni–Ca–Al(8:72:20)	2.95	17.36	11	68.7
Ni–Ca–Al(8:67:25)	2.5	15.32	12.02	70.16
Ni–Ca–Al(8:62:30)	2.05	15.17	13.99	68.79
Ni–Ca–Al(8:57:35)	1.72	13	16.21	69.07
Ni–Al(8:98)	1.71	–	28.02	70.27
[a]Ni–Ca–Al(8:62:30)	1.93	11.66	18.32	68.09

[a] Catalyst used in steam reforming of toluene reaction at 650 °C for 24 h.
[b] Obtained from XPS analysis.

interactions between Ni species and support species were significantly enhanced during the reforming reaction. In addition, the molar composition of various surface species present in freshly reduced Ni/Al(8:92), Ni–Ca–Al and spent Ni–Ca–Al(8:62:30) catalysts are presented in Table 3. According to Table 3, the trend in the elemental compositions of Ca and Al of Ni–Ca–Al catalysts are similar to their nominal compositions, whereby moving from Ni–Ca–Al(8:72:20) to Ni–Ca–Al(8:57:35), both nominal and surface amount of Ca species were decreased while the amount of Al species were increased. This also suggests the homogeneity of Ni–Ca–Al catalysts prepared via HT-like precursors. On the other hand, the surface contents of Ni species were observed to be decreased slightly with decreasing Ca/Al content in the catalysts. It is also observed from Table 3 that the surface Ni content of Ni–Ca–Al(8:62:30) catalyst was slightly decreased for the spent catalyst after 23 h SRT reaction, which is also associated with increase in the surface Al species. This decrease in the surface Ni species is possible due to either agglomeration of Ni species (in Table 2) or partial encapsulation with Al species (in Fig. 11b). This decrease in the surface Ni content might cause the slight deactivation of Ni–Ca–Al(8:62:30) catalysts in SRT reaction over 24 h reaction time. Finally, together with TPR analysis and Ni 2p BE of Ni–Ca–Al catalysts, we can observe the homogeneity and Ca(Ni, Al)O solid solution forms for Ni–Ca–Al catalysts.

3.11. DT/TG analyses of spent catalysts

The nature and amount of carbon deposited and amount of CO_2 adsorbed over spent Ni–Ca(8:92), Ni–Al(8:92) and Ni–Ca–Al catalysts after SRT at 650 °C are measured using TGA/DTA analyses up to 900 °C in air. The reaction times of spent catalysts are shown in Fig. 3. The TGA and DTA profiles are presented in Fig. 12A and B, respectively. The TGA profile for spent Ni–Al(8:92) catalyst in Fig. 12A shows a single stage weight loss between 400 and 700 °C. At this temperature range, the DTA profile of Ni–Al(8:92) catalyst in Fig. 12B has an exothermic peak. Thus suggests that this weight loss corresponds to the oxidation of carbon species

Table 4
Carbon deposition rate and amount of CO_2 desorbed for spent catalysts determined by TGA analysis. Reaction condition: reaction temperature = 650 °C; toluene = 188 μmol min^{-1}; S/C = 1; He = 5357 μmol min^{-1}; W = 100 mg.

Catalyst	Carbon deposition rate (mg g^{-1} h^{-1})	Amount of CO_2 desorbed (%)
Ni/CaO(8:92)	130.4	15.1
Ni–Ca–Al(8:72:20)	25.1	17.5
Ni–Ca–Al(8:67:25)	6	17.9
Ni–Ca–Al(8:62:30)	2.5	12.6
Ni–Ca–Al(8:57:35)	15.1	9.9
Ni–Al(8:92)	45.3	–

deposited during the SRT reaction over Ni–Al(8:92) catalyst [53,54]. Similar kind of weight loss is also observed for all other catalysts in the temperature range of 400–650 °C. It could be caused by the oxidation of deposited carbon during SRT reaction. The amount of weight loss due to carbon deposited on all the spent catalysts was determined and summarized in Table 4. The results indicate that Ni–Ca–Al(8:62:30) catalyst possesses lower amount of carbon formation rate (ca. 2.5 mgC g − cat^{-1} h^{-1}) as compared to the carbon formation rate of Ni–Ca(8:92), Ni–Ca–Al(8:72:20), Ni–Ca–Al(8:67:25), Ni–Ca–Al(8:57:35), and Ni–Al(8:92) catalysts (ca. 130.4, 25.1, 6, 15 and 45 mgC g − cat^{-1} h^{-1}, respectively). It is also observed that all Ni–Ca–Al catalysts generally had lower carbon formation rates as compared to Ni–Ca(8:92) and Ni–Al(8:92) catalysts. Weight loss and its corresponding endothermic peak below 300 °C (in Fig. 12A and B, respectively) are observed for almost all the CaO containing catalysts, possibly due to the desorption of physisorbed water molecules, which could be adsorbed by the catalysts while collecting the sample after SRT reaction. Furthermore, in Fig. 12A and B, an endothermic weight loss between 600 °C and 750 °C temperature region has been observed for all CaO containing catalysts. This weight loss is due to the desorption of CO_2 species from decomposition of $CaCO_3$ species. The $CaCO_3$ species could be formed during the SRT reaction and the presence of $CaCO_3$ species was further confirmed through XRD patterns (in Fig. 8B) of spent Ni–Ca–Al catalysts. The amount of CO_2 desorbed on all the spent catalysts was determined and is also summarized in Table 4. This result indicates that the amount of CO_2 adsorbed during steam reforming reaction is considerably lower than the amount of CO_2 adsorbed over fresh catalysts. By combining these results with CO_2 – TPD results presented in Fig. 10, it can be concluded that the lowest carbon deposition rate on Ni–Ca–Al(8:62:30) catalyst is due to its highest basicity among all the other Ni–Ca–Al catalysts.

4. Conclusions

The Ni–Ca–Al catalyst prepared from hydrotalcite precursors with an optimum catalyst composition of Ni–Ca–Al(8:62:30) showed better catalytic performance for both the steam reforming of toluene and biomass reactions compared to all other catalysts. The superior catalytic performance of Ni–Ca–Al(8:62:30) catalyst over other catalysts is mainly due to its enhanced basic strength and resistance toward agglomeration during the steam reforming reaction at 650 °C. The bi-functional property of Ni–Ca–Al catalysts was also explored. CO_2 sorption study at 650 °C shows that Ni–Ca–Al(8:62:30) catalysts displays considerably stable CO_2 sorption behavior for up to 10 carbonation and de-carbonation cycles. The influence of CO_2 sorption ability of Ni–Ca–Al catalysts in enhancing the steam reforming of toluene reaction in terms of H_2 production rates and CO_2 selectivities is clearly observed based on the fact that all CaO containing catalysts generally obtained lower CO_2 selectivity than Ni–Al(8:92) catalysts. This suggests that the synergism between the active Ni phase and CaO phase in Ni–Ca–Al catalysts results in the bi-functional property of Ni–Ca–Al catalyst which in turn leads to promising performance in steam reforming of tar reaction. Finally, these hydrotalcite derived Ni–Ca–Al catalysts have a great potential for application in many other sorption enhanced processes involving the production of carbon dioxide.

Acknowledgements

The authors gratefully thank National University of Singapore and National Environmental Agency (NEA-ETRP Grant No. 1002114 and RP No. 279-000-333-490) for generously supporting this work.

Appendix A. Supplementary data

Supplementary data associated with this article can be found, in the online version, at http://dx.doi.org/10.1016/j.apcatb.2015.02.017.

References

[1] G.W. Huber, S. Iborra, A. Corma, Chem. Rev. 106 (2006) 4044–4098.
[2] X. Hu, G. Lu, Appl. Catal. B: Environ. 88 (2009) 376–385.
[3] P.J. Dauenhauer, B.J. Dreyer, N.J. Degenstein, L.D. Schmidt, Angew. Chem. 119 (2007) 5968–5971.
[4] D.P. Serrano, J. Aguado, J.M. Escola, ACS Catal. 2 (2012) 1924–1941.
[5] J.C. Serrano-Ruiz, J.A. Dumesic, Energy Environ. Sci. 4 (2011) 83–99.
[6] J.C.S. -Ruiz, R. Luque, J.A. A.S.-Escribano, Chem. Soc. Rev. 40 (2011) 5266–5281.
[7] J.A. Melero, J. Iglesias, A. Garcia, Energy Environ. Sci. 5 (2012) 7393–7420.
[8] D.M. Alonso, S.G. Wettstein, J.A. Dumesic, Chem. Soc. Rev. 41 (2012) 8075–8098.
[9] K.A. Magrini-Bair, S. Czernik, R. French, Y.O. Parent, E. Chornet, D.C. Dayton, C. Feik, R. Bain, Appl. Catal. A: Gen. 318 (2007) 199–206.
[10] Progress in Biomass Gasification: An Overview, in: K.I. Maniatis, V. Bridgwater (Eds.), Blackwell Science, London, 2001, pp. 1–31.
[11] A. Dorazio, A.D. Carlo, N. Dionisi, A.D. Era, F. Orecchini, Int. J. Hydrogen Energy 38 (2013) 13282–13292.
[12] Ashok, S. Kawi, ACS Catal. 4 (2014) 289–301.
[13] U. Oemar, M.L. Ang, W.F. Hee, K. Hidajat, S. Kawi, Appl. Catal. B: Environ. 148–149 (2014) 231–242.
[14] Y. Shen, K. Yoshikawa, Renew. Sustain Energy Rev 21 (2013) 371–392.
[15] Z. Zhao, N. Lakshminarayanan, J.N. Kuhn, A.S. -Naber, L.G. Felix, R.B. Slimane, C.W. Choi, U.S. Ozkan, Appl. Catal. A: Gen. 363 (2009) 64–72.
[16] T. Kimura, T. Miyazawa, J. Nishikawa, S. Kado, K. Okumura, T. Miyao, S. Naito, K. Kunimori, K. Tomishige, Appl. Catal. B: Environ. 68 (2006) 160–170.
[17] E.G. Baker, L.K. Mudge, M.D. Brown, Ind. Eng. Chem. Res. 26 (1987) 1335–1339.
[18] J. Ashok, S. Kawi, Int. J. Hydrogen Energy 38 (2013) 13938–13949.
[19] K. Nakamura, T. Miyazawa, T. Sakurai, T. Miyao, S. Naito, N. Begum, K. Kunimori, K. Tomishige, Appl. Catal. B: Environ. 86 (2009) 36–44.
[20] M. Koike, C. Ishikawa, D. Li, L. Wang, Y. Nakagawa, K. Tomishige, Fuel 103 (2013) 122–129.
[21] J. Ashok, M. Subrahmanyam, A. Venugopal, Int. J. Hydrogen Energy 33 (2008) 2704–2713.
[22] M.K.R. Reddy, Z.P. Xu, G.Q. (Max) Lu, J.C.D. da Costa, Ind. Eng. Chem. Res. 45 (2006) 7504–7509.
[23] W. Fang, S. Paul, M. Capron, F. Dumeignil, L.J. Duhamel, Appl. Catal. B: Environ. 152–153 (2014) 370–382.
[24] A. Aristizabal, S. Contreras, N. Barrabes, J. Llorca, D. Tichit, F. Medina, Appl. Catal. B: Environ. 110 (2011) 58–70.
[25] D. Li, L. Wang, M. Koike, Y. Nakagawa, K. Tomishige, Appl. Catal. B: Environ. 102 (2011) 528–538.
[26] D. Li, M. Koike, L. Wang, Y. Nakagawa, Y. Xu, K. Tomishige, ChemSusChem 7 (2014) 510–522.
[27] L. Wang, D. Li, H. Watanabe, M. Tamura, Y. Nakagawa, K. Tomishige, Appl. Catal. B: Environ. 150–151 (2014) 82–92.
[28] K. Takehira, T. Shishido, P. Wang, T. Kosaka, K. Takaki, J. Catal. 221 (2004) 43–54.
[29] L.B. Raberg, M.B. Jensen, U. Olsbye, C. Daniel, S. Haag, C. Mirodatos, A.O. Sjastad, J. Catal. 249 (2007) 250–260.
[30] R.G. Lopez, V.L. Parola, M.A. Pena, J.L.G. Fierro, Catal. Today 116 (2006) 289–297.
[31] M. Broda, A.M. Kierzkowska, D. Baudouin, Q. Imtiaz, C. Coperet, C.R. Muller, ACS Catal. 2 (2012) 1635–1646.
[32] G. Wu, C. Zhang, S. Li, Z. Huang, S. Yan, S. Wang, M. Xinbin, J. Gong, Energy Environ. Sci. 5 (2012) 8942–8949.
[33] L. Xu, H. Song, L. Chou, ACS Catal. 2 (2012) 1331–1342.
[34] I. Zamboni, C. Courson, D. Niznansky, A. Kiennemann, Appl. Catal. B: Environ. 145 (2014) 63–72.

[35] G. Guan, G. Chen, Y. Kasai, E.W.C. Lim, X. Hao, M. Kaewpanha, A. Abuliti, C. Fushimi, A. Tsutsumi, Appl. Catal B: Environ. 115–116 (2012) 159–168.
[36] J. Fermoso, F. Rubiera, D. Chen, Energy Environ. Sci. 5 (2012) 6358–6367.
[37] S. Tada, M. Yokoyama, R. Kikuchi, T. Haneda, H. Kameyama, J. Phys. Chem. C 17 (2013) 14652–14658.
[38] U. Oemar, P.S. Ang, K. Hidajat, S. Kawi, Int. J. Hydrogen Energy 38 (2013) 5525–5534.
[39] P.H. Chang, Y.P. Chang, S.Y. Chen, C.T. Yu, Y.P. Chyou, ChemSusChem 4 (2011) 1844–1851.
[40] C.C.-H. Wu, Y.-P. Chang, S.-Y. Chen, D.-M. Liu, C.-T. Yu, B.-L. Pen, J. Nanosci. Nanotechnol. 10 (2010) 4716–4720.
[41] Y. Sekine, D. Mukai, Y. Murai, S. Tochiya, Y. Izutsu, K. Sekiguchi, N. Hosomura, H. Arai, E. Kikuchi, Y. Sugiura, Appl. Catal. A: Gen. 451 (2013) 160–167.
[42] F.L. Chan, A. Tanksale, ChemCatChem 6 (2014) 2727–2739.
[43] K. Tasaka, T. Furusawa, A. Tsutsumi, Energy Fuels 21 (2007) 590–595.
[44] K. Tomishige, M. Asadullah, K. Kunimori, Catal. Surv. Asia 7 (2003) 219–233.
[45] H. Lu, A. Khan, P.G. Smirniotis, Ind. Eng. Chem. Res. 47 (2008) 6216–6220.
[46] B.B. Sakadjian, M.V. Iyer, H. Gupta, L.S. Fan, Ind. Eng. Chem. Res. 46 (2007) 35–42.
[47] Z.S. Li, N.S. Cai, Y.Y. Huang, Ind. Eng. Chem. Res. 45 (2006) 1911–1917.
[48] P. Gallezot, G. Bergeret, Handbook of Heterogeneous Catalysis, in: G. Ertl, H. Knozinger, F. Schuth, J. Weitkamp (Eds.), Wiley-VCH, 2010, pp. 738–765.
[49] C.K.S. Choong, Z. Zhong, L. Huang, Z. Wang, T.P. Ang, A. Borgna, J. Lin, L. Hong, L. Chen, Appl. Catal. A: Gen. 407 (2011) 145–154.
[50] Z.L. Zhang, X.E. Verykios, Catal. Today 21 (1994) 589–595.
[51] L. Pino, A. Vita, F. Cipiti, M. Lagana, V. Recupero, Appl. Catal. B: Environ. 104 (2011) 64–73.
[52] Hand Book of X-ray Photoelectron Spectroscopy, in: C.D. Wagner, W.M. Riggs, L.E. Davis, J.F. Moulder, G.E. Muilenberg (Eds.), PerkinElmer Corporation, 1979, pp. 76–80.
[53] J.J. Spivey, G.W. Roberts, C.A. Querini, Catalysis 17 (2004) 166–209.
[54] B.D. Gould, X. Chen, J.W. Schwank, Appl. Catal. A: Gen. 334 (2008) 277–290.